

AD-A063 330

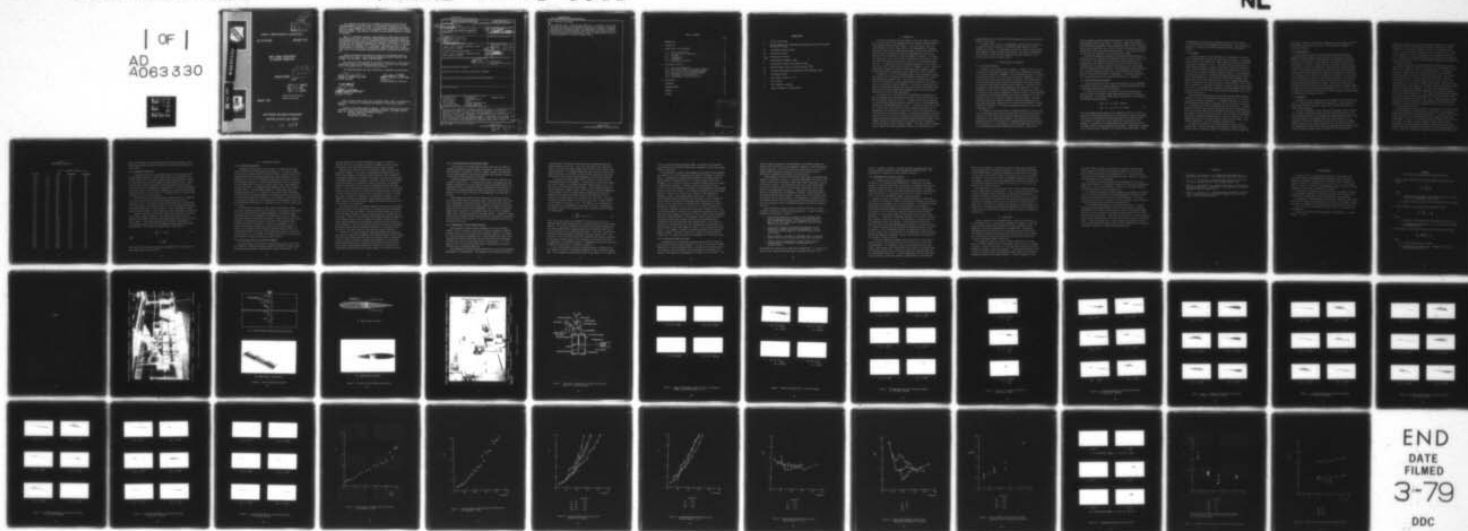
FRANK J SEILER RESEARCH LAB UNITED STATES AIR FORCE --ETC F/G 20/4
WATER TUNNEL MEASUREMENTS OF UNSTEADY SEPARATION.(U)
DEC 78 M S FRANCIS, J D LANG, J E KEESEE

UNCLASSIFIED

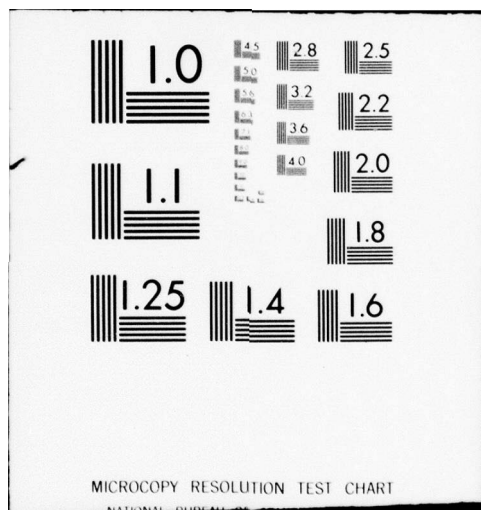
FJSRL-TR-78-0011

NL

| OF |
AD
A063 330



END
DATE
FILMED
3-79
DDC





AD A063330

DDC FILE COPY.



Now
LEVEL II

FRANK J. SEILER RESEARCH LABORATORY

SRL-TR-78-0011

DECEMBER 1978

WATER TUNNEL MEASUREMENTS
OF UNSTEADY SEPARATION

INTERIM REPORT

DDC
RECEIVED
JAN 17 1979
A

CAPT M. S. FRANCIS
MAJ J. D. LANG
CAPT J. E. KEESEE

APPROVED FOR PUBLIC RELEASE;
DISTRIBUTION UNLIMITED.

PROJECT 2307

AIR FORCE SYSTEMS COMMAND
UNITED STATES AIR FORCE

9 01 16 115

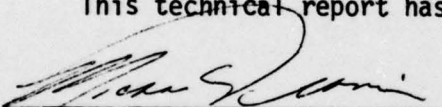
This document was prepared by the Mechanics Division, Directorate of Aerospace-Mechanics Sciences, Frank J. Seiler Research Laboratory, United States Air Force Academy, Colorado. The research was conducted under Project Work Unit Number 2307-F1-34, An Investigation of the Flow Dynamics of Unsteady Separated Regions. Capt Michael S. Francis was the Project Engineer in charge of the work.

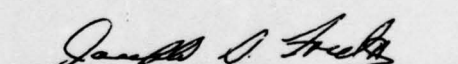
When U.S. Government drawings, specifications or other data are used for any purpose other than a definitely related Government procurement operation, the Government thereby incurs no responsibility nor any obligation whatsoever, and the fact that the Government may have formulated, furnished or in any way supplied the said drawings, specifications or other data is not to be regarded by implication or otherwise, as in any manner licensing the holder or any other person or corporation or conveying any rights or permission to manufacture, use or sell any patented invention that may in any way be related thereto.

Inquiries concerning the technical content of this document should be addressed to the Frank J. Seiler Research Laboratory (AFSC), FJSRL/NH, USAF Academy, Colorado 80840. Phone AC 303-472-3122.

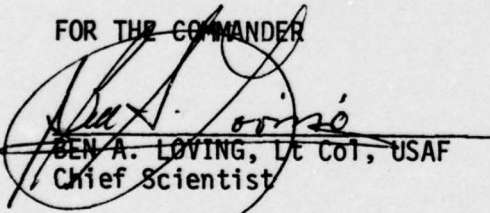
This report has been reviewed by the Chief Scientist and is releasable to the National Technical Information Service (NTIS). At NTIS it will be available to the general public, including foreign nations.

This technical report has been reviewed and is approved for publication.


MICHAEL S. FRANCIS, Capt, USAF
Project Engineer


JOSEPH S. FORD II, Lt Col, USAF
Director
Aerospace-Mechanics Sciences

FOR THE COMMANDER


BEN A. LOVING, Lt Col, USAF
Chief Scientist

Copies of this report should not be returned unless return is required by security considerations, contractual obligations, or notice on a specific document.

Printed in the United States of America. Qualified requestors may obtain additional copies from the Defense Documentation Center. All others should apply to: National Technical Information Service
5285 Port Royal Road
Springfield, Virginia 22161

UNCLASSIFIED

SECURITY CLASSIFICATION OF THIS PAGE (When Data Entered)

REPORT DOCUMENTATION PAGE		READ INSTRUCTIONS BEFORE COMPLETING FORM															
1. REPORT NUMBER 24 F SRL-TR-78-0011 AD A-	2. GOVT ACCESSION NO.	3. RECIPIENT'S CATALOG NUMBER															
4. TITLE (and Subtitle) 6 WATER TUNNEL MEASUREMENTS OF UNSTEADY SEPARATION	5. TYPE OF REPORT & PERIOD COVERED 9 Interim Report Oct 1977-Oct 1978																
7. AUTHOR(s) 10 Capt Michael S./Francis, Maj James D./Lang Capt John E./Keese	6. PERFORMING ORG. REPORT NUMBER																
9. PERFORMING ORGANIZATION NAME AND ADDRESS Frank J. Seiler Research Laboratory (AFSC) USAF Academy, CO 80840	8. CONTRACT OR GRANT NUMBER(s)																
11. CONTROLLING OFFICE NAME AND ADDRESS Frank J. Seiler Research Laboratory (AFSC) USAF Academy, CO 80840	10. PROGRAM ELEMENT, PROJECT, TASK AREA & WORK UNIT NUMBERS 16 DRS 61102F 2307-F1-34 17 F1																
14. MONITORING AGENCY NAME & ADDRESS (if different from Controlling Office) 12 53 p.	12. REPORT DATE 11 Dec 1978																
	13. NUMBER OF PAGES 49																
	15. SECURITY CLASS. (of this report) UNCLASSIFIED																
15a. DECLASSIFICATION/DOWNGRADING SCHEDULE																	
16. DISTRIBUTION STATEMENT (of this Report) Approved for public release; distribution unlimited.																	
17. DISTRIBUTION STATEMENT (of the abstract entered in Block 20, if different from Report)																	
18. SUPPLEMENTARY NOTES																	
19. KEY WORDS (Continue on reverse side if necessary and identify by block number) <table border="0"> <tr> <td>Unsteady Flow</td> <td>Aerodynamics</td> <td>Hydrogen Bubble</td> </tr> <tr> <td>Flow Separation</td> <td>Flow Visualization</td> <td></td> </tr> <tr> <td>Water Tunnel</td> <td>Airfoil</td> <td></td> </tr> <tr> <td>Fluid Mechanics</td> <td>Unsteady Separated Flow</td> <td></td> </tr> <tr> <td>Oscillating Spoiler</td> <td>Unsteady Separation</td> <td></td> </tr> </table>			Unsteady Flow	Aerodynamics	Hydrogen Bubble	Flow Separation	Flow Visualization		Water Tunnel	Airfoil		Fluid Mechanics	Unsteady Separated Flow		Oscillating Spoiler	Unsteady Separation	
Unsteady Flow	Aerodynamics	Hydrogen Bubble															
Flow Separation	Flow Visualization																
Water Tunnel	Airfoil																
Fluid Mechanics	Unsteady Separated Flow																
Oscillating Spoiler	Unsteady Separation																
20. ABSTRACT (Continue on reverse side if necessary and identify by block number) <p>The results of experiments in which a controlled region of flow separation was generated downstream of an oscillating fence-type spoiler located on one surface of an airfoil are discussed. The experiments were conducted in a low speed water tunnel under incompressible flow conditions over a wide range dimensionless frequencies and Reynolds numbers. High speed motion pictures and still photographs of hydrogen bubbles formed at surface mounted electrodes were used to obtain data regarding the shape and growth characteristics of</p> <p style="text-align: right;">→ next page</p>																	

DD FORM 1 JAN 73 1473 EDITION OF 1 NOV 65 IS OBSOLETE

UNCLASSIFIED

SECURITY CLASSIFICATION OF THIS PAGE (When Data Entered)

319 920

UNCLASSIFIED

SECURITY CLASSIFICATION OF THIS PAGE (When Data Entered)

20. Abstract (continued)

the separation zone. Under certain conditions, an energetic vortex-like structure was observed to form behind the spoiler and evolve in a manner determined by the Reynolds number and dimensionless frequency parameters. Observations of flow development reveal that the global structure of the separated region during the formation process is qualitatively similar to the one encountered in classical dynamic stall.

UNCLASSIFIED

SECURITY CLASSIFICATION OF THIS PAGE (When Data Entered)

TABLE OF CONTENTS

	Page
NOMENCLATURE	2
I. INTRODUCTION	3
II. DESCRIPTION OF THE EXPERIMENT.	4
II.1 Facility Description.	4
II.2 Flow Visualization Techniques	5
II.3 The Model	6
II.4 Instrumentation	7
II.5 Photography	7
II.6 Experimental Conditions	10
III. DISCUSSION OF RESULTS.	11
III.1 Steady Flow Separation.	11
III.2 Oscillation Effects at Low Reynolds Numbers	11
III.3 Flow Description at High Reynolds Numbers	13
III.4 Measurement of Vortex Growth Parameters	13
III.5 Flow Reversal Near the Surface.	15
III.6 Measurements of Convective Velocity	17
IV. CONCLUSIONS.	18
REFERENCES	20
ACKNOWLEDGEMENTS	21
APPENDIX	22
FIGURES.	23

ADMISSION IN	
RTS	WAVE NUMBER <input checked="" type="checkbox"/>
ODC	REF. NUMBER <input type="checkbox"/>
REMARKS	<input type="checkbox"/>
JUSTIFICATION	
BY	
SIGNATURE/INITIALS	
DATE	
TIME	
A	

NOMENCLATURE

c	airfoil chord length
h	maximum height of the separated region measured relative to the adjacent airfoil surface
h_s	instantaneous spoiler height
h_{s0}	mean spoiler height
h_{smax}	maximum spoiler height
k	dimensionless frequency, $\omega c/2U_\infty$
ℓ	instantaneous length of the separated region
Re	Reynolds number, based on the airfoil chord, $\frac{\rho U_\infty c}{\mu}$
U_c	characteristic velocity associated with the separated region
U_∞	freestream velocity
ϕ	phase angle of motion (= ωt)
ρ	fluid density
μ	fluid kinematic viscosity
ω	angular frequency of spoiler motion

I. INTRODUCTION

Flight vehicle maneuvers at high angles of attack can result in dynamic stall or other similar flow phenomena related to unsteady separation which can cause departure from controlled flight or, in the very least, alter the predicted behavior of the flight vehicle. The implementation of avoidance techniques or the possible productive employment of the positive features of these flows must be preceded by a detailed knowledge of the role of the dominant physical mechanisms in their development and behavior. The experiments described in this report involve a controlled flow separation in which the separation location was fixed with respect to the freestream coordinate direction. The separated region was produced downstream of an oscillating fence-type spoiler located at the mid-chord of a symmetric airfoil. Controlled experimental parameters included the freestream velocity (Reynolds number), spoiler mean height and amplitude, and the spoiler oscillation frequency.

Observations of the flow development reveal that the sequence of events associated with this particular flow environment are qualitatively similar to that encountered in dynamic stall. To aid in the investigation of the details of flow behavior, it was determined that a definitive flow visualization of the separation zone was necessary. In an effort to employ the best possible visualization technique for this type of problem, experiments using water as the flow medium with minute hydrogen bubbles as the flow markers were found to be most suitable (Reference 1).

Of significance in the selection of the experimental conditions was a desire to compare and correlate the visual results with available data from other experiments (References 2 and 3). The water tunnel facility employed for the experiments described below is located at the U.S. Army Aeromechanics Laboratory at the NASA/Ames Research Center. It provided a capability for the exact duplication of the dynamic similarity parameters previously used. A geometrically similar model to the one used in the earlier experiments was fabricated for the new flow environment. An additional advantage of the water tunnel facility was its ability to achieve low freestream speeds resulting in nominally laminar flow conditions associated with the separated region. These laminar flow results might be useful for a comparison with corresponding calculations based on simple analytical models. The current effort, therefore, seeks to examine the detailed geometric features of a generalized form of

unsteady separation and to verify or refute previous conceptions regarding the nature of these flows.

The report details two sets of experiments conducted at flow conditions representing opposing extremes in the Reynolds number capability of the experimental facility. The experiments which involve laminar flow conditions were conducted at Reynolds numbers below 20,000. The remaining measurements which describe a highly turbulent separation zone were conducted in the Reynolds number range of 200,000 - 800,000.

II. DESCRIPTION OF THE EXPERIMENT

II.1 Facility Description

Experiments were conducted in the .2 meter x .3 meter (8 inch x 12 inch) closed circuit, continuous flow water tunnel at the Aeromechanics Laboratory, U.S. Army R&T Laboratories (AVRADCOM) at the Ames Research Center in California. A complete description of this facility can be found in Reference 4. The unit contains approximately 4,000 cubic meters of water and, with the exception of the fiber glass contraction section and the plexiglass test section windows, is constructed from type 304 stainless steel (Figure 1). Continuous flow is provided by a three-bladed impeller powered by a DC motor using a silicon controlled rectifier drive. Steady flow velocities continuously variable from 0-6 meters per second could be obtained in the test section. Flow straightening and turbulence reduction was affected by two sets of honeycomb, 4 sections of screening, and a 10:1 contraction upstream of the test section. Two large tanks are available for storing a portion of the water withdrawn from the tunnel when making model changes and for dissolving fresh chemicals to combat biological contaminants. A filtration system was designed to remove contaminants down to 5 μ m.

The presence of cavitation-induced air bubbles presented a serious limitation on the maximum usable speed in the test section since they can severely interfere with the viewing of the smaller bubbles which are intentionally generated for flow visualization purposes. The problem can be minimized by subjecting the water in the tunnel to a vacuum and extracting the majority of the dissolved air. In the present case, this was accomplished with a series of three polypropylene venturi tubes used as aspirators. Water from an

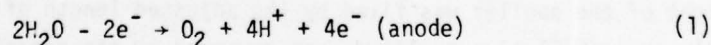
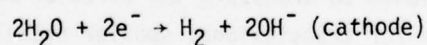
external source was passed through each venturi at a rate that produced a 0.6-atmosphere vacuum at each throat. The venturi throats were joined by a common tube that was attached to the plexiglass air dome on top of the tunnel. Degassing was accomplished prior to the initiation of photographic studies to provide the best possible visualization conditions. It was especially necessary for the tests conducted at the higher Reynolds numbers.

Following the degassing procedure, the tunnel was pressurized using a regulated source of compressed air connected by tubing to the air dome on top of the tunnel. The increase of pressure in the water (differential to 1 atmosphere) had the effect of reducing the size of all bubbles that were formed during a test, whether they were due to cavitation or to the gases that were produced during electrolysis. The advantages of tunnel pressurization, including reduced cavitation bubble volume and decreased buoyancy effects, are more fully discussed in Reference 1. The results presented in this study were obtained with a tunnel pressurization of 1 atmosphere.

II.2 Flow Visualization Techniques

The basic technique for flow visualization employed in this experiment involved the generation of hydrogen bubbles from surface mounted electrodes on the model using the process of electrolysis.

By placing two electrodes in an aqueous solution and maintaining a constant electrical potential between them, gaseous bubbles are formed at each electrode. This chemical process known as electrolysis is described by the following reaction formulas:



Since the hydrogen bubbles formed at the cathode during this reaction are smaller than the oxygen bubbles which are simultaneously formed at the anode, the model's surface mounted electrodes were used as the cathode and their size carefully tailored to yield the desired flow visualization bubble geometry. A suspension bolt located downstream, below the model and out of the camera field of view was maintained as the anode. Oxygen bubbles generated at this electrode were, therefore, not viewed during the experiment. Bubble

size depended on the electrolytic conductivity of the solution and the electrical potential applied between the two electrodes. This voltage level was used as a variable to regulate the bubble density for photographic purposes.

II.3 The Model

The model employed in these experiments was a NACA 0012 airfoil fabricated of aluminum which horizontally spanned the test section. A fence-type spoiler located at mid-chord on one (upper) surface was capable of sinusoidal oscillation at frequencies to 10 Hz. The spoiler was also constructed of aluminum and was located in a groove in the airfoil surface which was teflon lined. Twelve electrodes of varying lengths and orientation were located along the upper surface of the model as shown in Figure 2. These electrodes consisted of 0.05 mm thick platinum ribbon sandwiched between small sheets of nylon insulating material. The resultant assemblies were imbedded in the model using an epoxy filler material so that a single exposed edge (approximately 13 mm long) served as the active part of each electrode. After installation of these units, the model surface was finished to reduce surface roughness. A No. 30 insulated wire was soldered to each electrode and the ensemble of wires passed out of the model interior through an attachment point in the plexiglass viewing wall.

The sinusoidal pitching motion of the spoiler was generated through an interface to the oscillation mechanism used by McCroskey, et. al., in their experiments described in Reference 1. A flywheel, connecting rod, and rack and gear mechanism functioned to transform the circular motion of a DC motor to a reciprocating motion for translational spoiler oscillations. The mean height of the spoiler was fixed by the adjusted length of the connecting rod, while the oscillation amplitude was governed by the radial station selected on the flywheel at which the rod was connected. This combination of adjustments provided for oscillation amplitudes up to $\pm .240$ cm ($\pm .095$ inches). The flywheel was driven by a DC motor through a belt and pulley system, and the speed was governed by a silicon controlled rectifier drive.

The model was supported at both sides of the test section by four retaining pins. Spoiler oscillation was effected by a rotating rod which extended spanwise through the interior of the model on which spur gears had

been welded. Miniature racks rigidly attached to the spoiler were then driven by the rotary oscillations of this rod. The airfoil/spoiler geometry is described in Figure 3.

II.4 Instrumentation

Controls were available for selecting tunnel dynamic pressure, the frequency of model oscillation, and the location and intensity of bubble generation. Other electronics were available for synchronizing the cameras to the motion of the model. A disk geared to the flywheel axis was used to close photocell circuits at integer levels per revolution (usually once/rev). A resultant pulse served to energize the strobe and/or to release the camera shutter. The actuation phase angle over a cycle of motion was continuously selectable from 0-360 degrees and was adjusted by rotating a dial attached to the synchronizing disk. Another disk geared to the flywheel axis was used to close the photocell circuits at a rate of 90 per revolution. This provided pulses which could be summed over a fixed period of time to obtain the frequency at which the spoiler was oscillating. The signal was also used to generate the numerical display of the spoiler phase angle at 4 degree intervals. The image of this display was redirected through a series of mirrors so that the cumulative distance to the film plane of the high speed movie camera placed it within the critical depth of field.

II.5 Photography

Two types of camera systems were used to document the flow visualization results. They provided the capability of obtaining (1) single exposures for both frozen element and path line studies, and (2) high-speed movies for detailed motion analysis.

The still photographic system consisted of an automatic 70 mm film magazine, a bellows type focusing body, and a high light gathering 240 mm lens (f4.5 minimum) coupled with an electronically controlled aperture and shutter (1/60 sec minimum). This composite camera (a Coleman Phototronic) was mounted on a rigid 9 cm diameter pipe so that the film plane was located a nominal distance of 152 cm from the center of the test section (Figure 4). This combination of lens and film plane-to-subject distance was found to offer the best compromise between image size, depth of field and perspective

distortion. The black and white film used in this camera was a high-speed medium-grain roll film which yields normal density exposures at f8 when processed in a high-contrast developer at 85°F and at a machine rate of 1.5 m/s. The minimization of geometric distortion created with this system in conjunction with a similar flow geometry was documented by McAlister, et. al. (Reference 1). Based on these results, it was concluded that photographs of the flow field could be analyzed without applying any correction for perspective distortion.

The second system was a high-speed, precision motion picture camera (DBM Millikan) capable of indexing 16 mm film at up to 500 frames/sec (using positive pin registration) with $\pm 1.5\%$ speed stability. This camera was mounted on a rotatable arm which allowed the lens axis to be coaxially positioned in front of the lens of the first camera system. The resulting distance between the film plane and the center of the test section was nominally 86 cm. At this focusing range a 50 mm lens was found to cover approximately 21 cm, or almost 1.4 airfoil chord lengths. Preliminary tests indicated that a minimum setting of 128 frames/sec would be required for motion analysis of various flow phenomena. The actual frame rate employed for a given set of experimental conditions depended on both freestream speed and spoiler oscillation frequency (k). Table 1 details the photographic parameters used with the highly light sensitive ASA 400 film and less sensitive color film for the experiments discussed below. Due to lighting conditions, camera limitations, and film sensitivity, it was found that the ASA 400 B/W film required a one-stop push during development, while the less sensitive color film required a two-stop push.

Both photographic systems were used in conjunction with a lighting system in which the bubbles were illuminated by a narrow sheet of light directed through the overhead test section window (Figure 5). Two baffles were used to control the width of the light beam as well as to ensure a parallel beam configuration. The path of the beam was oriented 10 degrees from the plane of the bubbles to provide a necessary component of back lighting without compromising the required vertical spread of illumination above the model. Both continuous and intermittent flash sources of light were employed with the systems. Continuous lighting was provided by two lamps totaling 1000 watts.

Table 1
Experimental Conditions

<u>Re x 10⁻⁵</u>	<u>k</u>	Motion Picture		
		<u>Film</u>	<u>Aperature</u>	<u>Frame Rate</u>
2.46	0.0	B/W	f2	128
2.46	0.85	B/W	f1.6	250
2.87	0.0	B/W	f2	128
2.87	0.05	B/W	f2	128
2.87	0.1	B/W	f2	128
2.87	0.2	B/W	f2	128
2.87	0.3	B/W	f2	128
2.87	0.5	B/W	f2	128
4.10	0.0	B/W	f2	128
4.10	0.1	B/W	f1.6	250
4.10	0.3	B/W	f1.6	250
4.10	0.5	B/W	f1.6	250
5.54	0.0	B/W	f1.6	250
5.54	0.1	B/W	f1.6	250
5.54	0.3	B/W	f1.6	250
6.15	0.3	B/W	f1.6	500
0.10	2.2	Color	f1.6	64
0.10	3.7	Color	f1.6	64
0.10	5.4	Color	f1.6	64
0.10	7.9	Color	f1.6	64
0.20	0.8	Color	f1.6	64
0.20	1.5	Color	f1.6	64
0.20	1.8	Color	f1.6	64
0.30	0.0	Color	f1.6	64
0.30	0.5	Color	f1.6	64
0.30	1.0	Color	f1.6	64
0.30	2.1	Color	f1.6	64
0.05	0.0	Color	f1.6	64

When an instantaneous visualization of the flow field was needed at a pre-selected phase angle of spoiler oscillation, a 30 mm long xenon strobe tube was activated.

II.6 Experimental Conditions

As indicated earlier, two complimentary sets of flow conditions representing different extremes in tunnel speed capability were employed. The minimum speed at which the tunnel conditions could be operated was limited by the error tolerance in bubble trajectory caused by buoyancy forces. Lower Reynolds numbers could be employed in conjunction with increasing spoiler oscillation frequency to demonstrate flow domination by increasingly energetic separation vortices. Dimensionless frequencies (k) up to 6.00 were generated at Reynolds numbers as low as 17,000. All documented laminar flow tests were conducted for k -values exceeding unity.

Higher Reynolds number experiments were conducted to effect a comparison with earlier surface pressure field data obtained by Lang and Francis (References 2 and 3) and current wind tunnel experiments now being conducted at the USAF Academy. Accordingly, actual oscillation frequencies were varied to generate dimensionless " k "-values from 0.1 - 0.85 in the Reynolds number range of 200,000 - 800,000. Table 1 details the exact combinations investigated.

The data discussed in the following sections were obtained for a single set of spoiler geometry parameters. The spoiler mean height was set at 0.240 cm (0.095 inches), while the peak-to-peak amplitude was fixed at 0.480 cm (0.190 inches). The minimum spoiler height, therefore, corresponded to a flush surface condition and the fully extended distance equaled the peak-to-peak amplitude. The oscillation characteristic is then given as

$$\frac{h_s}{h_{s0}} = 1 - \cos \omega t \quad (2)$$

where

$$\omega = \frac{2U_\infty k}{c}$$

The airfoil angle-of-attack was fixed at zero degrees (0°), and the spoiler mean height (h_{s0}) was set at 0.24 cm.

III. DISCUSSION OF RESULTS

III.1 Steady Flow Separation

Although the primary intent of this report is to describe the global effects resulting from forced spoiler oscillations, it is useful to briefly discuss the flow character with fixed spoiler height. With the spoiler fully retracted (flush) and low Reynolds number free stream conditions, a thick boundary layer on the airfoil surface was observed to evolve into a trailing edge separation condition. Periodically-shed vortices, similar in character to those associated with the classic Karman vortex street, were detected in the near wake region. The separation zone adjacent to the airfoil surface is characterized by a low energy eddy bounded by a laminar shear layer (the separated boundary layer). An increase in the Reynolds number (freestream velocity) results in rearward movement of the separation point and a thinning of the upstream boundary layer (Figure 6). The frequency of the shed vortices is observed to increase while their characteristic size decreases. Also, the discrete shedding characteristic is observed to evolve to a more random, turbulent nature.

An extension of the spoiler to even a small but measurable distance resulted in detectable separation at the spoiler. The character of the separation region was observed to be somewhat dependent on the Reynolds number (freestream velocity) but appeared to be turbulent for the entire range of conditions examined in the present experiment. Increasing the spoiler height resulted in a perceptible increase of the length of the separated region. With the spoiler fully extended ($h_s = 0.480$ cm), reattachment or, more properly, confluence was observed to occur well into the wake region. An increase in the Reynolds number under these conditions had the effect of increasing the mixing in the shear layer between the separation zone and the outer potential flow. In addition, the energy (rotation rate) of the eddy was also observed to increase with Reynolds number (Figure 7).

III.2 Oscillation Effects at Low Reynolds Numbers

When the spoiler was oscillated in simple harmonic motion, even at very low frequencies, unsteady effects were observed to completely dominate other physical mechanisms commonly associated with steady flow conditions. The

resultant separation at low Reynolds numbers appeared to be laminar in character with an almost perfect cylindrically symmetric vortex structure originating at the spoiler and convecting along the airfoil surface.

Results from a typical cycle of oscillation for these conditions are presented in Figure 8. This series of photographs graphically depicts the formation and movement of the primary vortex structure. Not so apparent is the extremely energetic flow reversal which occurs during the initial stages of formation on the spoiler upstroke. A backflow into the region immediately behind the spoiler and up along the aft face of the spoiler is redirected rearward at the spoiler tip along with fluid emanating from the upstream region. A vortex-like structure results which appears to move as a solid body along the airfoil surface at a fraction of the freestream speed. The number of vortex structures which can exist over the surface of the airfoil at any given time is primarily a function of the dimensionless frequency. As the frequency is increased, one observes a longer effective residence time in terms of spoiler oscillation periods, thereby allowing more vortices to exist on the airfoil at any given time.

Also apparent at these low Reynolds numbers is the presence of secondary structures which also are vortex-like but are formed near the trailing edge due to roll-up of the shear layer. They are not formed directly by spoiler motion but appear related to a spoiler induced shear layer instability (like "tripping"). They are strong functions of both Reynolds number and dimensionless frequency (Figure 9), and can apparently interact strongly with the primary vortex depending on their relative location and the flow conditions during generation. Using high speed motion pictures, one might either observe the primary vortex ingest the secondary structure, or an interaction which culminates in the rapid breakup of both structures through turbulence.

Virtually all of the low Reynolds number measurements were obtained at high values of dimensionless frequency, and these measurements strongly support the notion that unsteady separation does not generally involve a growing and shrinking bubble as previously conceptualized (Reference 3), but may more properly be characterized by a coherent vorticity-bearing region which can grow, diffuse, and eventually convect into the wake of the airfoil while simultaneously affecting the local surface loading in a significant fashion.

III.3 Flow Description at High Reynolds Numbers

Visualization of the higher Reynolds number flows does not reveal as coherent a structure as that observed in the laminar, low speed case due to the high levels of turbulence. One does, however, observe a qualitatively similar growth progression involving an energetic flow reversal followed by an observable rotating, eddy-like structure.

A complete sequence of events for several sets of flow conditions are provided in Figures 10-15. In viewing these results, one observes that the geometric characteristics of the separation zone are measurable despite the detrimental effects of turbulent mixing on the quality of visualization. A differentiation between steady and unsteady flow effects at these Reynolds numbers is not as apparent from the still photographs as from the motion pictures.

Mixing between the potential flow region and the circulating region behind the spoiler appears to be quite strong in the outer shear layer interface. Reattachment is observed initially to occur on the airfoil surface during the initial stages of the spoiler upstroke, but extends into the wake region during mid-cycle and on the downstroke. Even in these high Reynolds number cases, the nature of the separated region does not fully resemble a "bubble" which grows and contracts as previously thought. Although the bubble concept might be employed to describe the growth of the separation zone during the initial part of the upstroke, it is not a valid characterization for the remainder of the cycle.

III.4 Measurement of Vortex Growth Parameters

Data provided by hydrogen bubbles generated by the long electrodes (numbers 1 and 2 in Figure 2) can be used to establish geometric parameters relating to the size of the primary vortex structure, especially its length (ℓ), and an aspect ratio parameter (h/ℓ). Both parameters were found to be reasonably well defined during that portion of the cycle where reattachment occurred on the airfoil surface (early part of the upstroke). It is this segment of the cycle during which the "bubble" characterization discussed previously has its greatest credibility.

The assessment of the region growth characteristics using direct geometric measurements is straightforward. The separation zone boundary was observed to

be well defined for moderate and high oscillation frequencies during the upstroke portion of the cycle. This can be attributed to the stabilizing effect of the relatively high rotation rates existing in this region at the higher frequencies. The boundary between the vorticity-bearing zone and the potential flow was less distinct at low oscillation rates due to the lower mean rotation rates and the increased dominance of turbulent fluctuations.

It is useful to discuss these results in terms of a comparison with corresponding steady flow parameters. A possible way to display this comparison in this instance is to observe the bubble length parameter, $2\ell/c$, as a function of the instantaneous spoiler height. The non-linear character of this relationship as shown in Figure 16 for one set of conditions immediately invites comparison with the linear behavior between spoiler height and separated region length postulated for steady flow (References 2 and 3). Although its behavior appears to be linear at first, the slope of the curve is observed to change abruptly at a relatively low value of spoiler height (in this example, at $h_s/h_{s_{\max}} \approx 0.17$). This behavior can be explained by considering the non-linear nature of the spoiler's motion. Differentiation of equation (2) leads to an expression for the instantaneous rate of change of spoiler height:

$$h_s \equiv \frac{dh_s}{dt} = \omega h_{s0} \sin \omega t \quad (3)$$

Early in the cycle, the rate of movement of the spoiler is slow so the separated region length characteristic can be approximated by its quasi-steady behavior. As the spoiler approaches its quarter cycle height (maximum rate), non-linear unsteady effects begin to dominate the fluid motion resulting in locally different rates of separation zone growth. The scatter in the data as the spoiler height approaches its maximum value (phase angle = 180°) is due primarily to the lack of definition of the separation zone geometry, again due to the highly turbulent nature of the structure at this point in the cycle. For comparison, a corresponding graph of a nondimensional separation zone length parameter with phase angle is presented in Figure 17.

A lag in the length of the vorticity-bearing region is observed to be a much stronger function of dimensionless frequency (k) than of Reynolds number (Re). This is apparent from comparing Figure 18 with Figure 19. For specified

values of spoiler height and Reynolds number, the length of the separation zone decreases with increasing dimensionless frequency (k) during the upstroke segment of the cycle.

The variation of an aspect ratio parameter associated with the separation zone geometry (h/ℓ) with instantaneous phase angle is displayed in Figures 20 and 21. As expected, the strong rotation evident in this region during the initial stages of formation results in a relatively large value for this parameter. This is especially true at low spoiler heights and for high values of dimensionless frequency. Resultant diffusion and convection of the vorticity in this zone results in a decrease in this parameter as the structure grows over the airfoil surface. This observed 'stretching' of the shear layer geometry is noted to vary primarily as a function of the dimensionless frequency. Changes in the region geometry due to the 3:1 variation in Reynolds number examined here appear to be negligible as shown in Figure 20. The variation of the aspect ratio parameter with dimensionless frequency, however, is more significant as is apparent from an examination of Figure 21. One observes a decrease in (h/ℓ) as the spoiler is raised, followed by an increase and a subsequent leveling off as the spoiler continues to be raised. The initial decrease in the value of the aspect ratio parameter occurs as the separation zone elongates and flattens in a similar manner to that encountered under quasi-steady conditions. The subsequent increase observed during the 'maximum oscillation rate' portion of the cycle can be attributed to a tightening of the vortex structure from unsteady effects. As the spoiler approaches its maximum height, the rate again decreases and the aspect ratio again decreases as the flow attempts to "catch up" to its steady flow configuration. This sequence of events is observed consistently for all Reynolds numbers examined. The overall effect of an increase in the dimensionless frequency is to increase the value of this parameter for a given phase angle.

III.5 Flow Reversal Near the Surface

An examination of flow reversal occurring near the airfoil surface was made utilizing three electrodes (numbers 10, 11 and 12 in Figure 2) oriented perpendicular to the freestream direction. Observation of the phase angle at which reversal occurred provided a direct and graphic illustration of the passage of the separation zone boundary as it moved aft on the airfoil. The

nature of reversal observed in the experiments at low Reynolds numbers was found to differ significantly from comparable situations in the high Reynolds numbers experiments. While this trend can be expected due to the values of Reynolds number employed, the behavior must also be attributed to the differences in dimensionless frequency for the two cases.

A representative variation of the reversal phase angle with dimensionless frequency is depicted in Figure 22. Note that the parameter described in this figure is actually the difference in phase angle between electrodes 11 and 12 on the airfoil surface. One observes here that, at a given location behind the spoiler, reversal occurs at a larger value of phase angle with larger values of the dimensionless frequency, k . The value of the reversal phase angle was not determined to be a detectable function of Reynolds number for the range of Reynolds number examined. A definitive, distinct reversal onset was observed only during the upstroke. An intermittency in reversal due to the turbulent nature of the flow characterized the downstroke/wash-off part of the cycle and made any form of quantitative graphical presentation extremely difficult.

The characteristic sequence of events leading to reversal at a given electrode is generalized in the following description. A specific example is presented for comparison in Figure 23.

- a. As the spoiler begins to rise from its fully retracted (flush with the surface) location, no effect is initially observed on the flow downstream location. This represents definitive evidence of the lag in region growth described by Lang and Francis (Reference 3) and others.
- b. As the spoiler reaches a prescribed height dependent on the dimensionless frequency and other flow parameters, an almost sinusoidal instability appears in the flow streaming aft from the electrode.
- c. Shortly thereafter, the periodic disturbance turns to turbulence characterized by mixing with the outer layer above the surface.
- d. Finally, after a few more degrees of phase change, the flow reverses abruptly, followed by a sloshing motion due to turbulent mixing.

These events are observed over a wide range of frequencies. It is the initial reversal that is measured and described in the graphs discussed in this

section. In general, reversal is observed to begin just behind the spoiler and extend downstream toward the trailing edge with increasing time. This characteristic is common to all flow situations observed.

III.6 Measurements of Convective Velocity

In a previous report which suggested a mass transfer model for the description of the separation zone (Reference 3), a measure of the growth employed in analytical modeling was the concept of a convective flow velocity. Although the data described in this report reject the concept of a growing separation "bubble" in favor of a vortex-oriented description of the separated region, the concept of a characteristic velocity still retains validity at least as far as the high Reynolds number cases are concerned.

Attempts to measure the length of the separated region in steady flow failed due to the presence of extensive turbulent mixing between the separation zone and the outer potential flow in these situations. For unsteady flow cases and moderate to high frequencies, an accurate definition of convective velocity was obtained by comparing flow photographs at various phase angles. One solution for this velocity was obtained by comparing the phase angle difference for flow reversal between two electrodes having a known physical separation, x . Observation of the phase difference at which reversal occurred then provided a characteristic time. The calculation of convective velocity then proceeds as shown in the Appendix. Another equivalent solution for convective velocity resulted from computing the length of the separated region as a function of phase angle and calculating an appropriate slope as shown in the Appendix. Since the chordwise location of separation was fixed at the spoiler in these cases, the correlation of the reattachment location with time provided the necessary information. Results from both types of calculations are provided in Figures 24 and 25.

A conclusion immediately apparent from the examination of these data is that the value of the convective velocity is some fractional value of the freestream speed. This parameter is observed to decrease with increasing values of the frequency while leveling off as the value of k approached unity. This parameter was not found to vary significantly with Reynolds number over the range examined (Figure 25). It must be emphasized that these data represent an "average" value of the convective speed variable and are therefore

useful only for parametric comparisons since the driving motion responsible for the unsteadiness is non-linear (sinusoidal). A more detailed definition of the variable might be obtained by measuring the local slope in the length vs phase angle characteristic (Figure 17) at various times during the formation process. The convective velocity calculated at low spoiler heights can be expected to differ from the value computed near mid-extension (h_{s0}) due to the non-linear character of the spoiler's motion in time. This result was addressed in a previous section.

The determination of a convective velocity in the low Reynolds number regime is complicated by several factors. Since the almost cylindrical vortex structure generated at these conditions for high values of dimensionless frequency is observed to detach from the spoiler and move aft, one is forced to observe the motion of the centroid of the vortex and not merely the variation of the reattachment location as is the case with the higher Reynolds number flow. The difficulty in making this observation is complicated by the appearance of the secondary structures discussed earlier which interfere and interact with the primary vortex structure tending to distort its geometry or destabilize it.

IV. CONCLUSIONS

Several observations can be summarized here based on the discussion in the preceding sections. The similarities between the sequence of events and global structure associated with dynamic stall and the separation zone generated in the present experiment can be re-emphasized. Although the observed progression of reversal aft on the airfoil surface in the present case appears to contradict observations associated with the onset of dynamic stall, the presence, growth and dispersion of the dominating vortex-like structure are features common to both flows.

This comparison aside, the results of these experiments cast serious doubt on a strict interpretation of the modified "bubble" concept of unsteady separation in favor of the notion of a vorticity-laden region which convects, deforms and diffuses as the cycle progresses. The coherence displayed by this structure is evident even at higher Reynolds numbers despite the presence of moderate turbulence levels during mid-cycle. It should, however, be noted

that earlier models derived from the idea of a separation "bubble" whose growth lagged the equivalent quasi-steady configuration still have some application during a portion of the upstroke part of the cycle so long as one realizes the limitations of those models and their inability to accurately describe the details of flow behavior.

The sequence of events associated with the generation of the primary large scale structure is significantly different for the low and high Reynolds number cases. The primary difference is the level of interaction (mixing) with the outer potential flow in the two cases.

The alternative methods of assessing separation zone growth with discrete point flow reversal measurements or direct measurement of the region length provide two comparable descriptions of the same phenomenon. The reversal properties are especially of interest in that this property is most indicative of the high energy associated with the unsteady effects.

A serious deficiency present in the current experiment is the lack of accurate quantitative measurements of the flow field variables. Accurate measurements of the velocity and/or vorticity fields in the separated region would be of great assistance in confirming the conclusions derived from the observations discussed above. They would also be useful for a direct comparison with available surface pressure field data which could be applied to analytical models. (These experiments are, in fact, currently being pursued by the F.J. Seiler Research Laboratory employing both hot-wire anemometry and laser Doppler velocimetry techniques for velocity field determination.)

REFERENCES

1. McAlister, K. W., and Carr, L. W., "Water Tunnel Experiments on an Oscillating Airfoil at $Re = 21,000$," NASA Tech. Memo. 78446, March 1978.
2. Lang, J. D., "The Dynamics of a Growing Separated Region on an Airfoil," F.J. Seiler Research Laboratory SRL-TR-75-0005, February 1975.
3. Lang, J. D., and Francis, M. S., "Dynamic Loading on an Airfoil Due to a Growing Separated Region," AGARD paper no. 27, Conference on Prediction of Aerodynamic Loading, September 1976.
4. Olsen, J. H., and Liu, H. T., "The Construction and Operation of a Water Tunnel in Application to Flow Visualization Studies of an Oscillating Airfoil," NASA CR-114696, May 1973.

ACKNOWLEDGEMENTS

The authors wish to express their appreciation and gratitude to the personnel of the U.S. Army Aeromechanics Laboratory, R and T Technology Laboratories (AVRADCOM) located at the Ames Research Center, especially the support provided by Dr. Ken McAlister, Dr. Larry Carr, Dr. W. J. McCroskey, and Mr. Art Cocco. We gratefully acknowledge the support provided by the NASA photographic support unit, especially Mr. Joe March.

The precision craftsmanship and expertise of Mr. Carl Geddes of the Frank J. Seiler Research Laboratory in fabricating the model and the water tunnel interface were indispensable to the success achieved in the experiment.

The personnel of the Department of Instructional Technology, USAF Academy, especially the Graphic Arts and Photographic Divisions, are commended for their fine work in the preparation of the figures and illustrations for this report.

Lastly, our thanks to Donna Weiss for her efforts in the preparation of this manuscript.

Portions of this report have been excerpted from Reference 1, including Figures 1, 4, and 5.

APPENDIX

Calculation and Interpretation of Convective Velocity

1. Method based on Comparison to Corresponding Steady Flow Event (Lang, Ref. 2)

$$\frac{U_c}{U_\infty} = \frac{x_t \cdot k}{2\pi(\phi_s - \phi)}$$

where

x_t - dimensionless reattachment location based on airfoil semi-chord at time, t (corresponding to phase angle, θ)

ϕ_s - steady flow phase angle at which reattachment occurs at location, x, t .

2. Direct Calculation using Instantaneous Reattachment Location

$$\frac{U_c}{U_\infty} = \frac{360}{\pi} \cdot \frac{k}{c} \cdot \frac{\Delta l}{\Delta \phi}$$

where

Δl - dimensional distance between two reattachment locations (x_1, x_2)

$\Delta \phi$ - corresponding phase difference ($\phi_2 - \phi_1$) associated with movement of reattachment point

3. Method Based on Flow Reversal Occurrence at Two Known Spatial Locations

$$\frac{U_c}{U_\infty} = \left(\frac{360}{\pi} \right) \frac{\Delta x}{c} \cdot \frac{k}{\Delta \phi}$$

where

Δx - distance between reversal locations

$\Delta \phi$ - dimensionless time (phase angle, in degrees) difference for which reversal occurs, $\phi_2 - \phi_1$

FIGURES

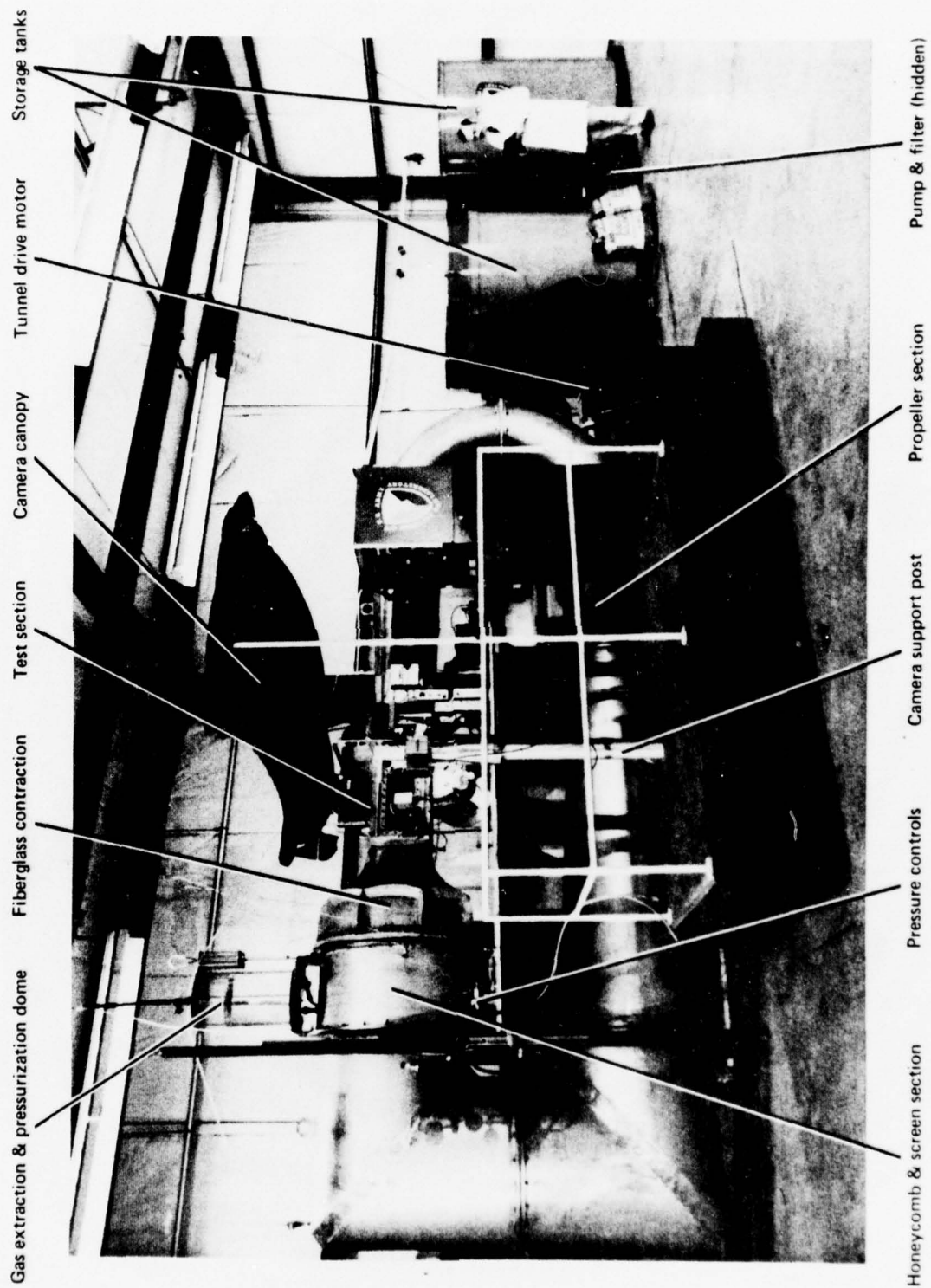
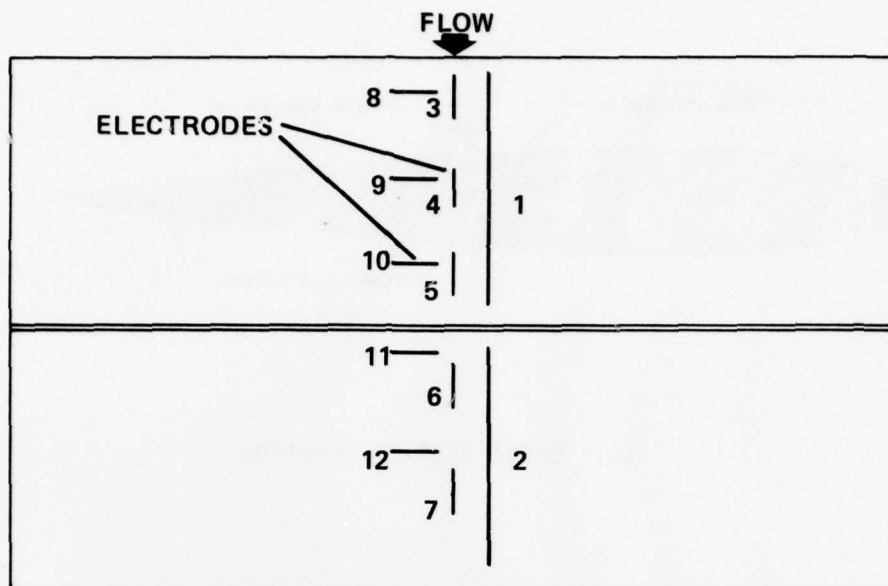
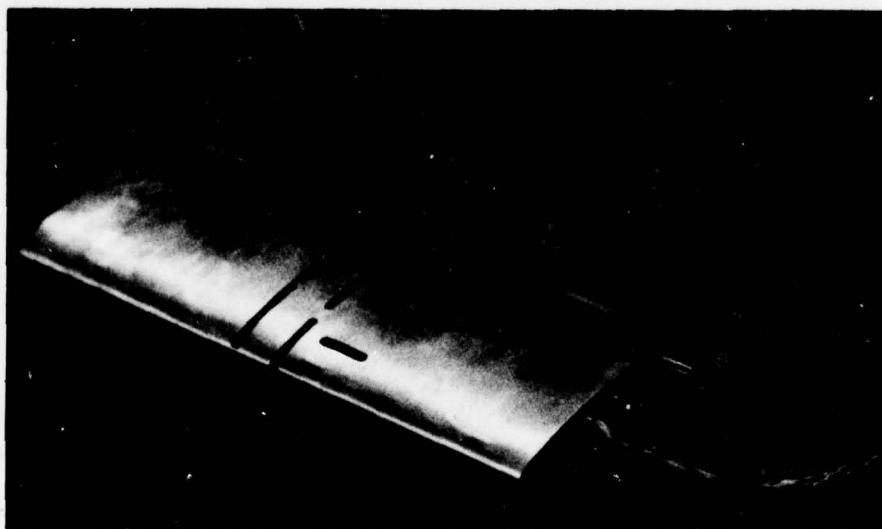


Figure 1. Aeromechanics Laboratory (AVRADCOM) 0.2m x 0.3m Water Tunnel

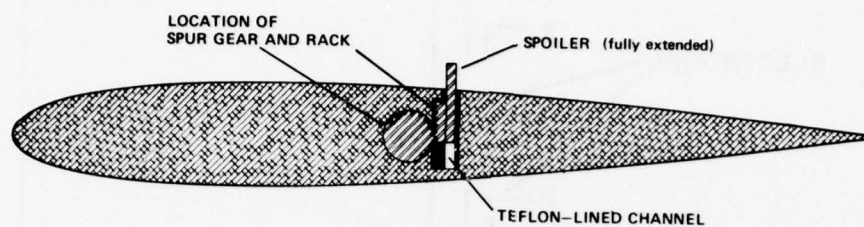


(a) Planform Sketch Showing Electrode Locations

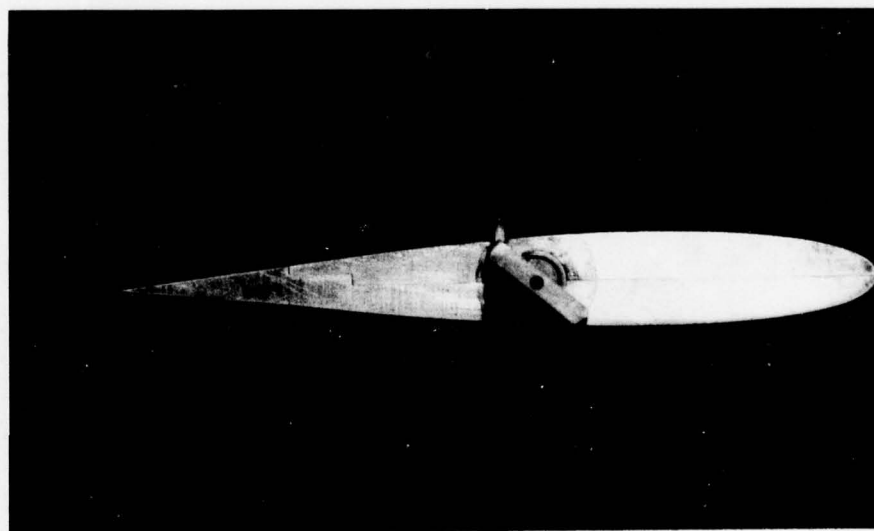


(b) Model Photo - Perspective

Figure 2. Airfoil Model with Spoiler



(a) Model Profile (sketch)



(b) Model Profile (photo)

Figure 3. Profile of Airfoil Model with Spoiler

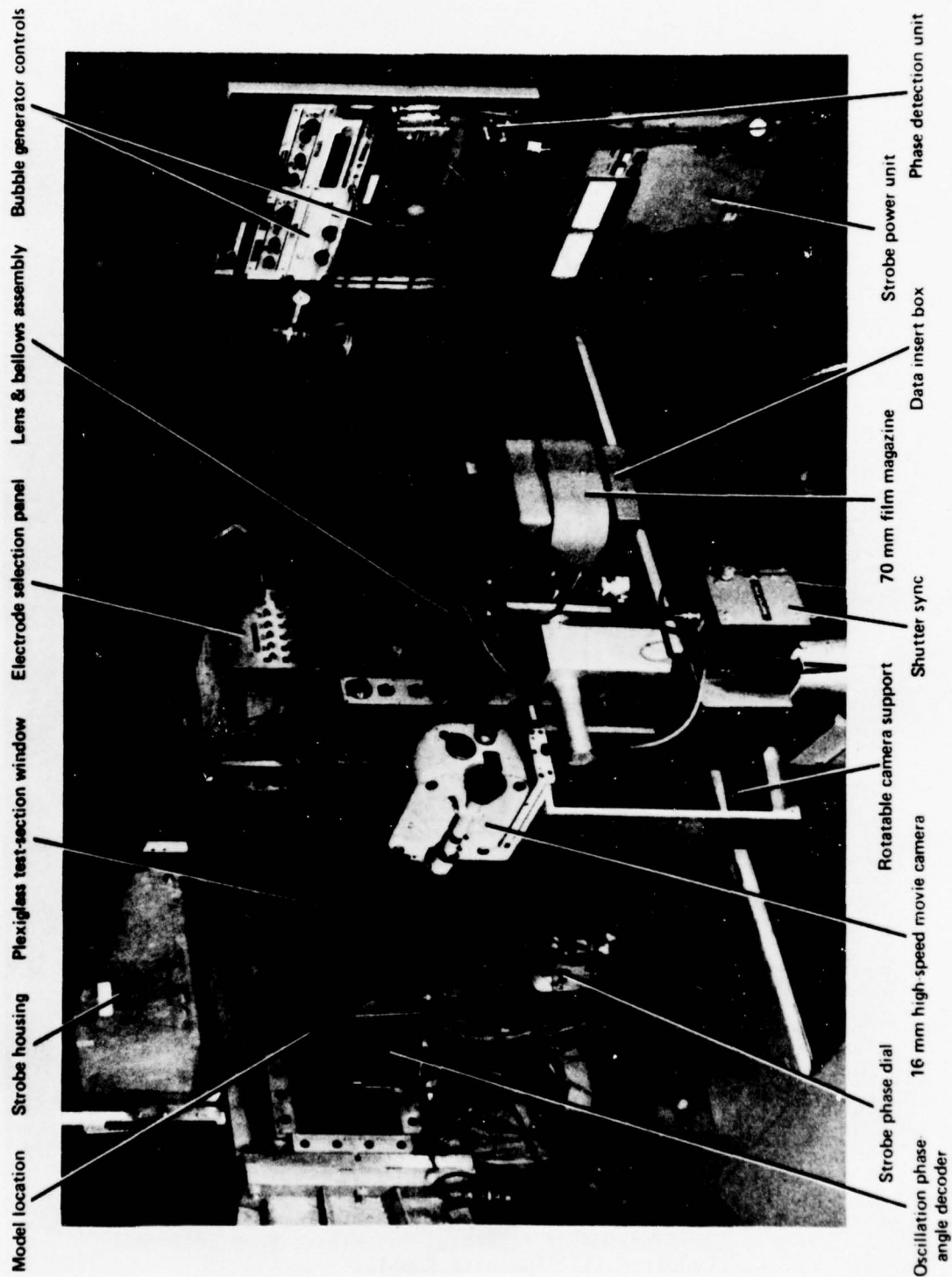


Figure 4. Instrumentation Layout

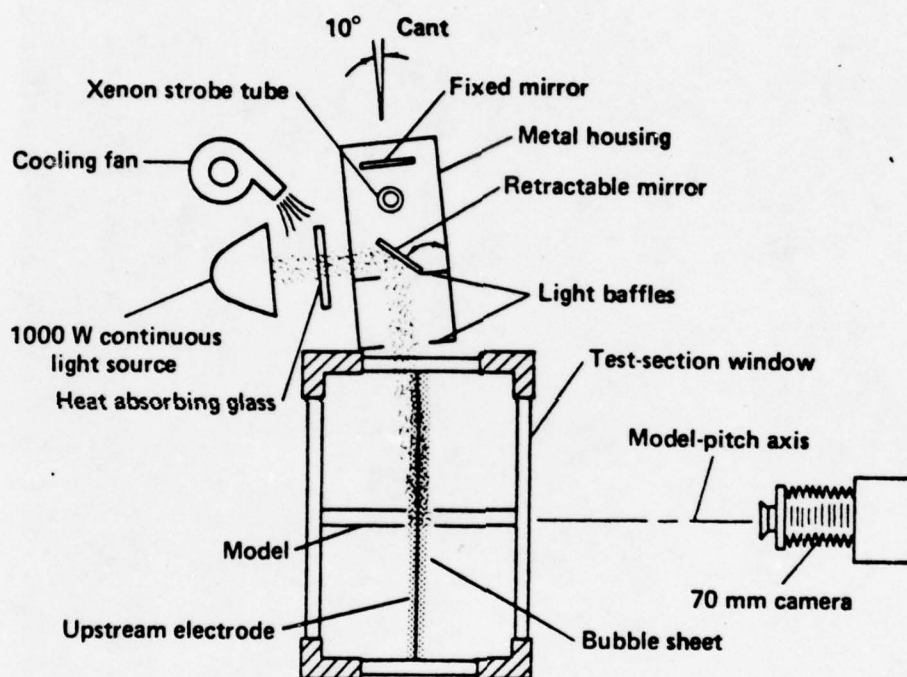


Figure 5. Orientation of Apparatus (as viewed from upstream)
Required to Illuminate Bubbles



(a) $Re \approx 5,000$



(b) $Re \approx 10,000$



(c) $Re \approx 20,000$



(d) $Re = 550,000$

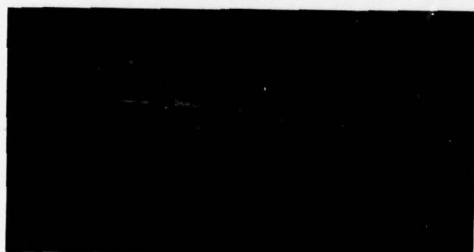
Figure 6. Steady Flow Boundary Layer Variation with Reynolds Number, Spoiler Retracted ($h_s = 0$)



(a) $h_s = h_{smax}$
 $Re \approx 10,000$



(b) $h_s = h_{smax}/2$
 $Re = 246,000$

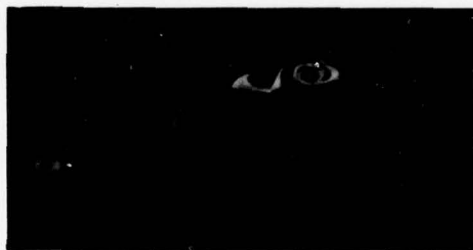


(c) $h_s = h_{smax}$
 $Re = 246,000$



(d) $h_s = h_{smax}$
 $Re = 510,000$

Figure 7. Steady Flow Separation - Spoiler Extended



(a) $\phi = 0^{\circ}$



(d) $\phi = 180^{\circ}$



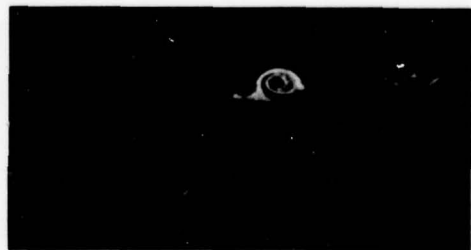
(b) $\phi = 60^{\circ}$



(e) $\phi = 240^{\circ}$



(c) $\phi = 120^{\circ}$



(f) $\phi = 300^{\circ}$

Figure 8. Unsteady Separation at Low Reynolds Number,
 $k = 3.70$, $Re \approx 10,000$



(a) $Re \approx 10,000$
 $k = 5.4$
 $\phi = 0^\circ$



(b) $Re \approx 10,000$
 $k = 5.4$
 $\phi = 220^\circ$



(c) $Re \approx 10,000$
 $k = 3.7$
 $\phi = 300^\circ$

Figure 9. Examples of Secondary Structure at Low Reynolds Numbers



(a) $\phi = 0^\circ$



(d) $\phi = 90^\circ$



(b) $\phi = 30^\circ$



(e) $\phi = 120^\circ$



(c) $\phi = 60^\circ$



(f) $\phi = 150^\circ$

Figure 10. Unsteady Separation at High Reynolds Number,
 $k = 0.85$, $Re = 246,000$



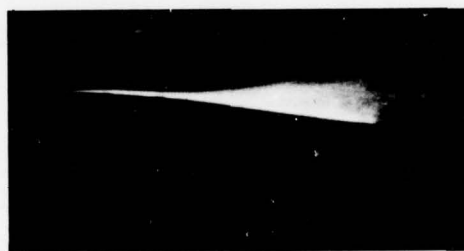
(g) $\phi = 180^\circ$



(j) $\phi = 270^\circ$



(h) $\phi = 210^\circ$



(k) $\phi = 300^\circ$

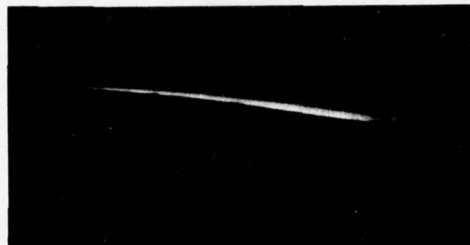


(i) $\phi = 240^\circ$

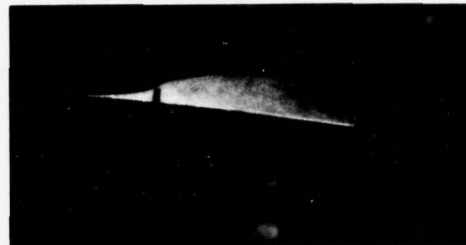


(l) $\phi = 330^\circ$

Figure 10 (cont). Unsteady Separation at High Reynolds
Number, $k = 0.85$, $Re = 246,000$



(a) $\phi = 0^\circ$



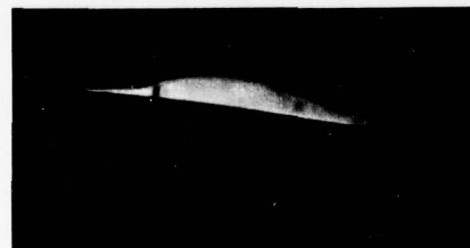
(d) $\phi = 180^\circ$



(b) $\phi = 60^\circ$



(e) $\phi = 240^\circ$

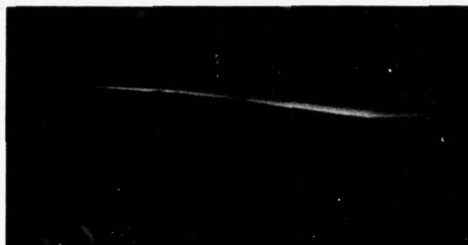


(c) $\phi = 120^\circ$



(f) $\phi = 300^\circ$

Figure 11. Unsteady Separation at High Reynolds Number,
 $k = 0.05$, $Re = 287,000$



(a) $\phi = 0^\circ$



(d) $\phi = 180^\circ$



(b) $\phi = 64^\circ$



(e) $\phi = 236^\circ$



(c) $\phi = 128^\circ$



(f) $\phi = 304^\circ$

Figure 12. Unsteady Separation at High Reynolds Number,
 $k = 0.30$, $Re = 287,000$



(a) $\phi = 0^{\circ}$



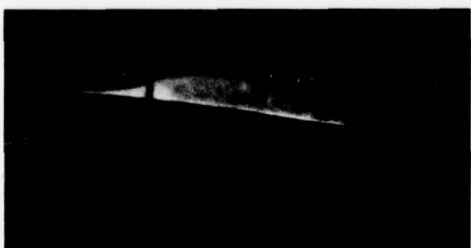
(d) $\phi = 176^{\circ}$



(b) $\phi = 64^{\circ}$



(e) $\phi = 240^{\circ}$

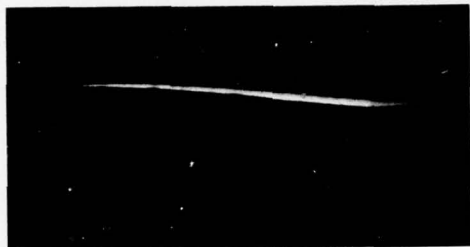


(c) $\phi = 128^{\circ}$



(f) $\phi = 304^{\circ}$

Figure 13. Unsteady Separation at High Reynolds Number,
 $k = 0.5$, $Re = 287,000$



(a) $\phi = 0^\circ$



(d) $\phi = 176^\circ$



(b) $\phi = 64^\circ$



(e) $\phi = 240^\circ$



(c) $\phi = 112^\circ$

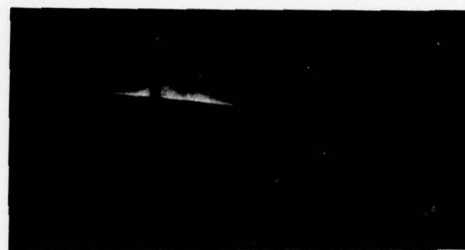


(f) $\phi = 304^\circ$

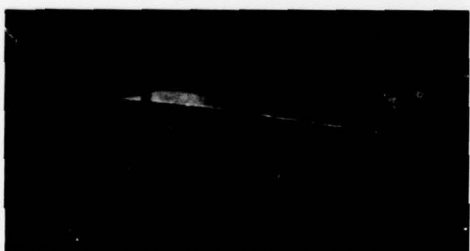
Figure 14. Unsteady Separation at High Reynolds Number,
 $k \approx 0.30$, $Re = 410,000$



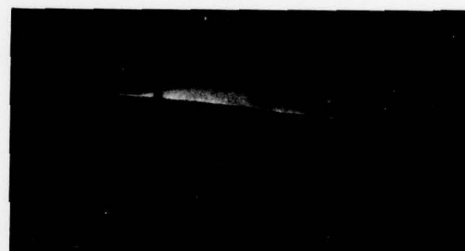
(a) $\phi = 0^\circ$



(d) $\phi = 180^\circ$



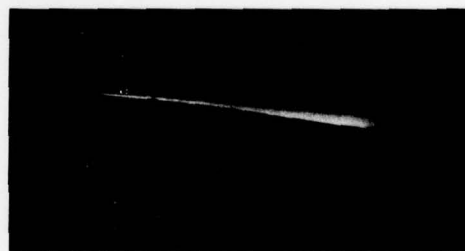
(b) $\phi = 64^\circ$



(e) $\phi = 240^\circ$



(c) $\phi = 112^\circ$



(f) $\phi = 304^\circ$

Figure 15. Unsteady Separation at High Reynolds Number,
 $k = 0.30$, $Re = 554,000$

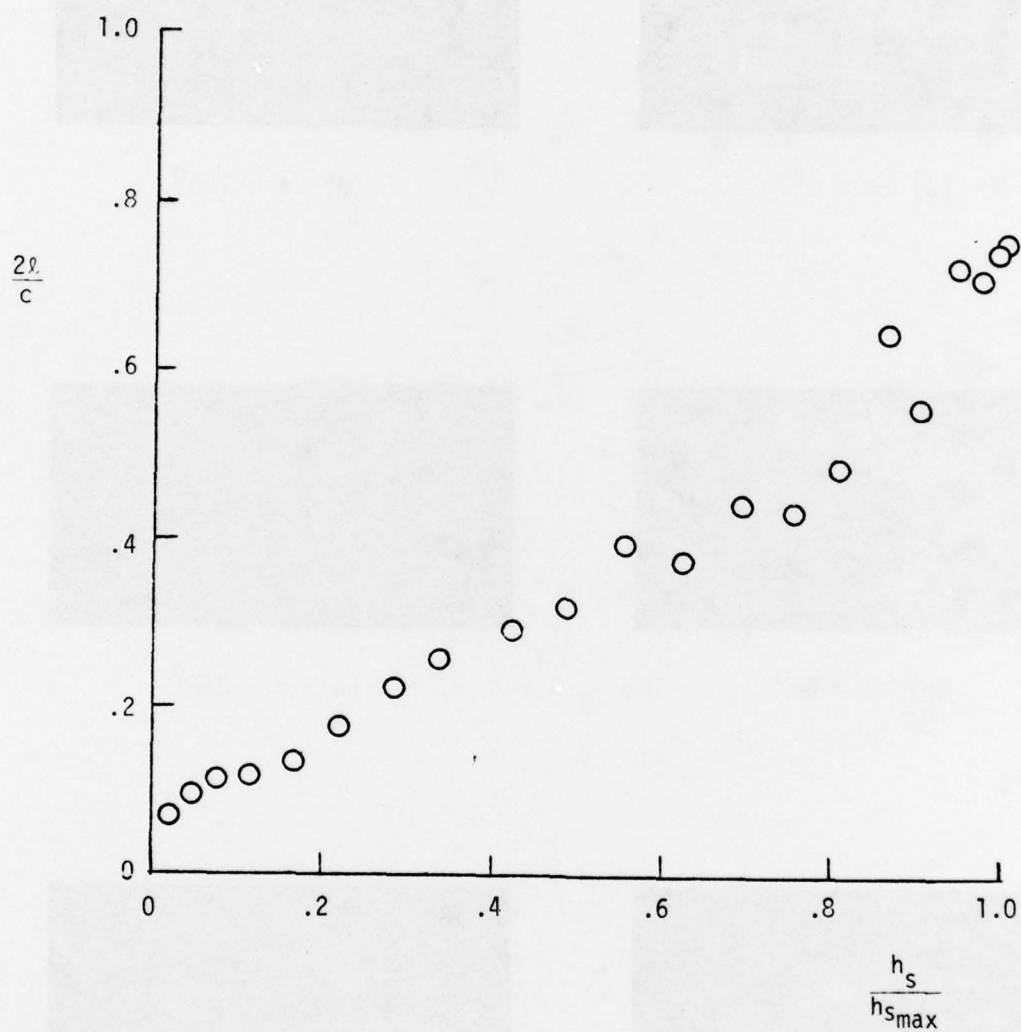


Figure 16. Bubble Length Variation with Spoiler Height,
 $Re = 246,000$, $k = 0.85$.

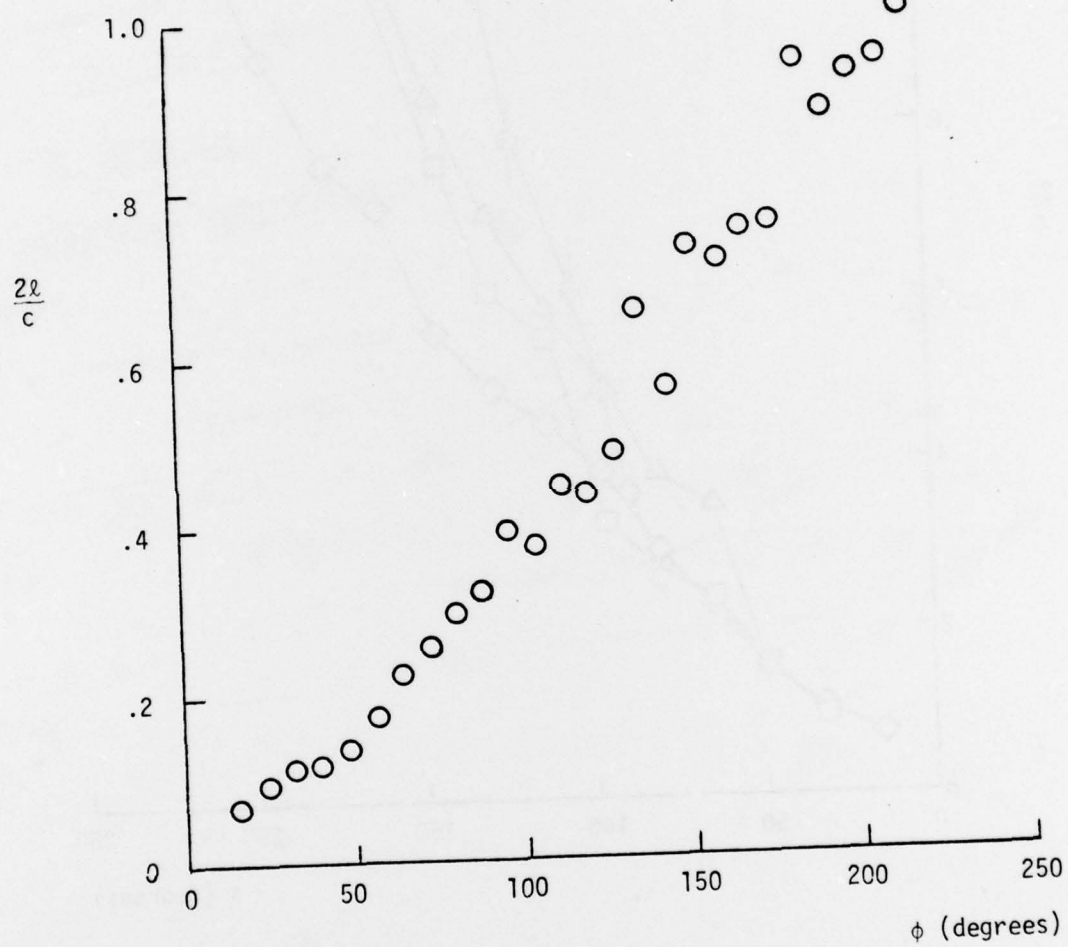


Figure 17. Separated Region Length Variation with Phase Angle
 $Re = 246,000$, $k = 0.85$.

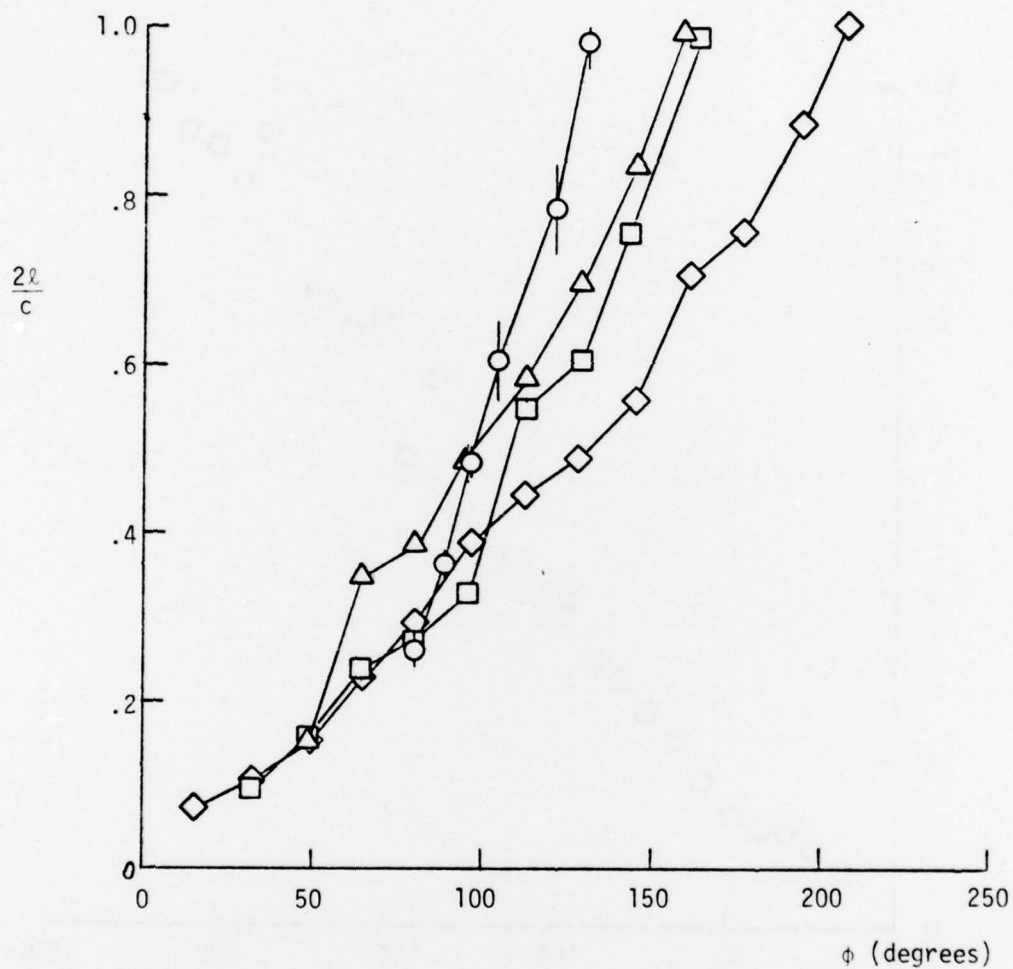


Figure 18. Separated Region Growth Variation with Dimensionless Frequency

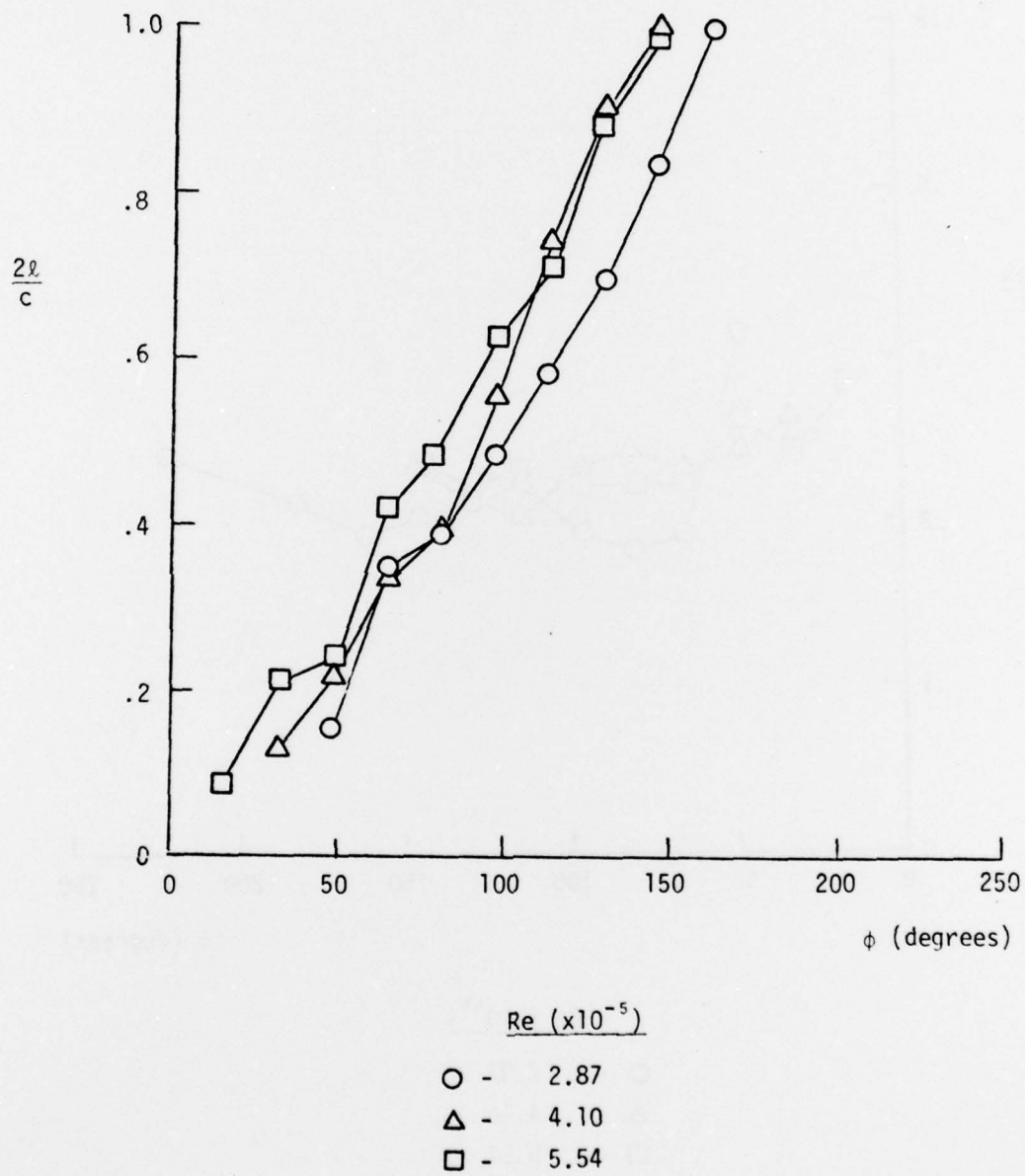
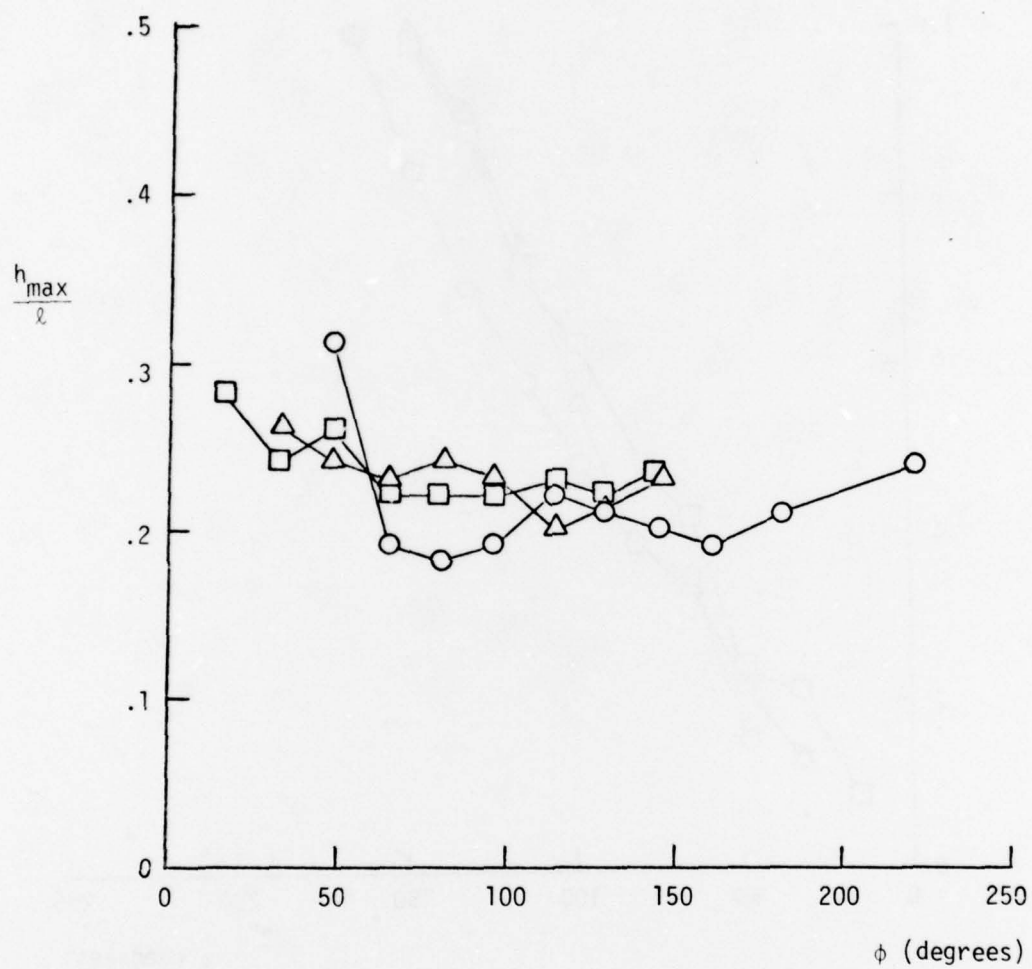


Figure 19. Separated Region Growth Variation with Reynolds Number, $k = 0.3$.



Re ($\times 10^{-5}$)

- - 2.87
- △ - 4.10
- - 5.54

Figure 20. Aspect Ratio Parameter Variation with Reynolds Number, $k = 0.30$.

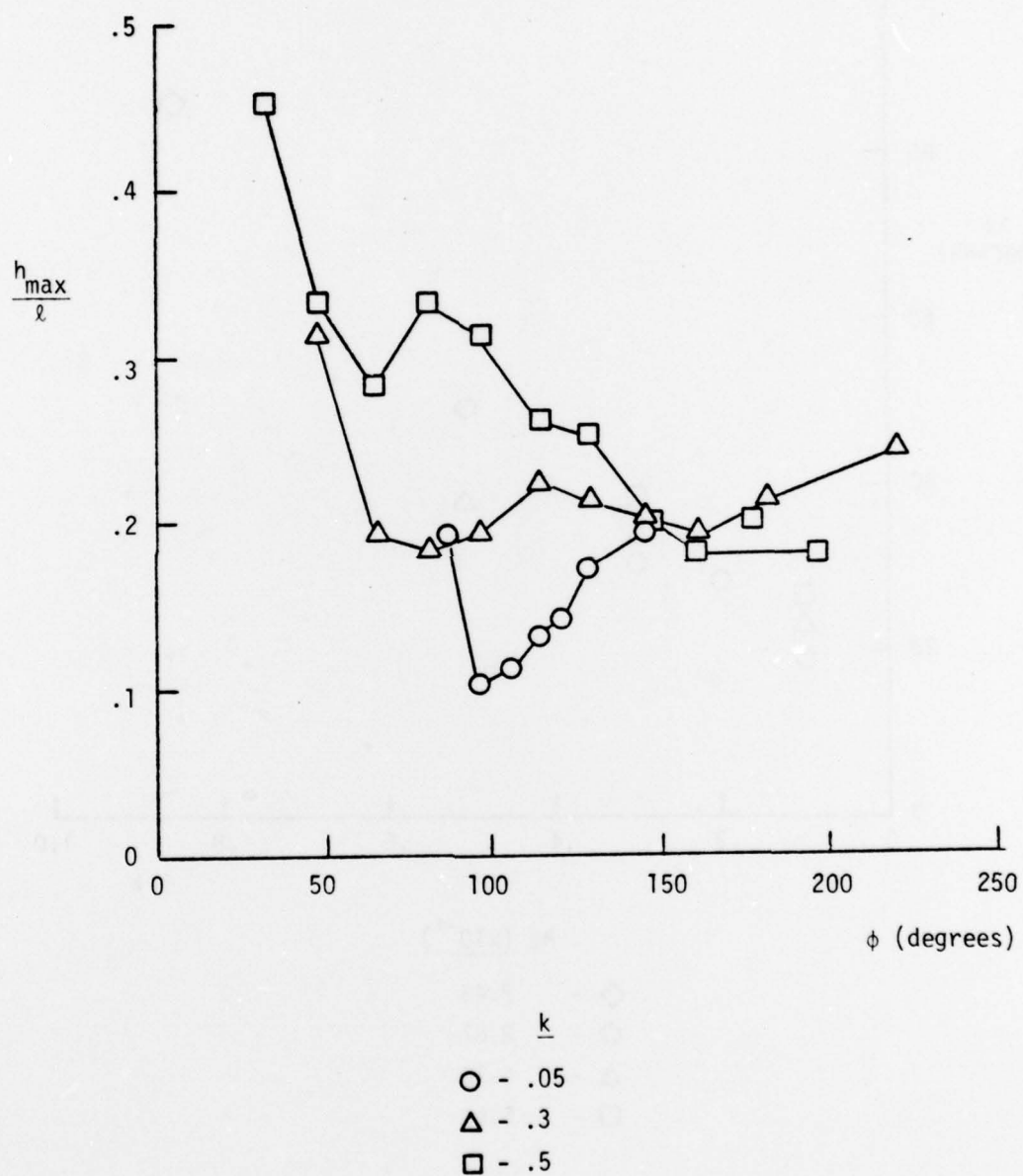


Figure 21. Aspect Ratio Parameter Variation with Dimensionless Frequency, $Re = 287,000$.

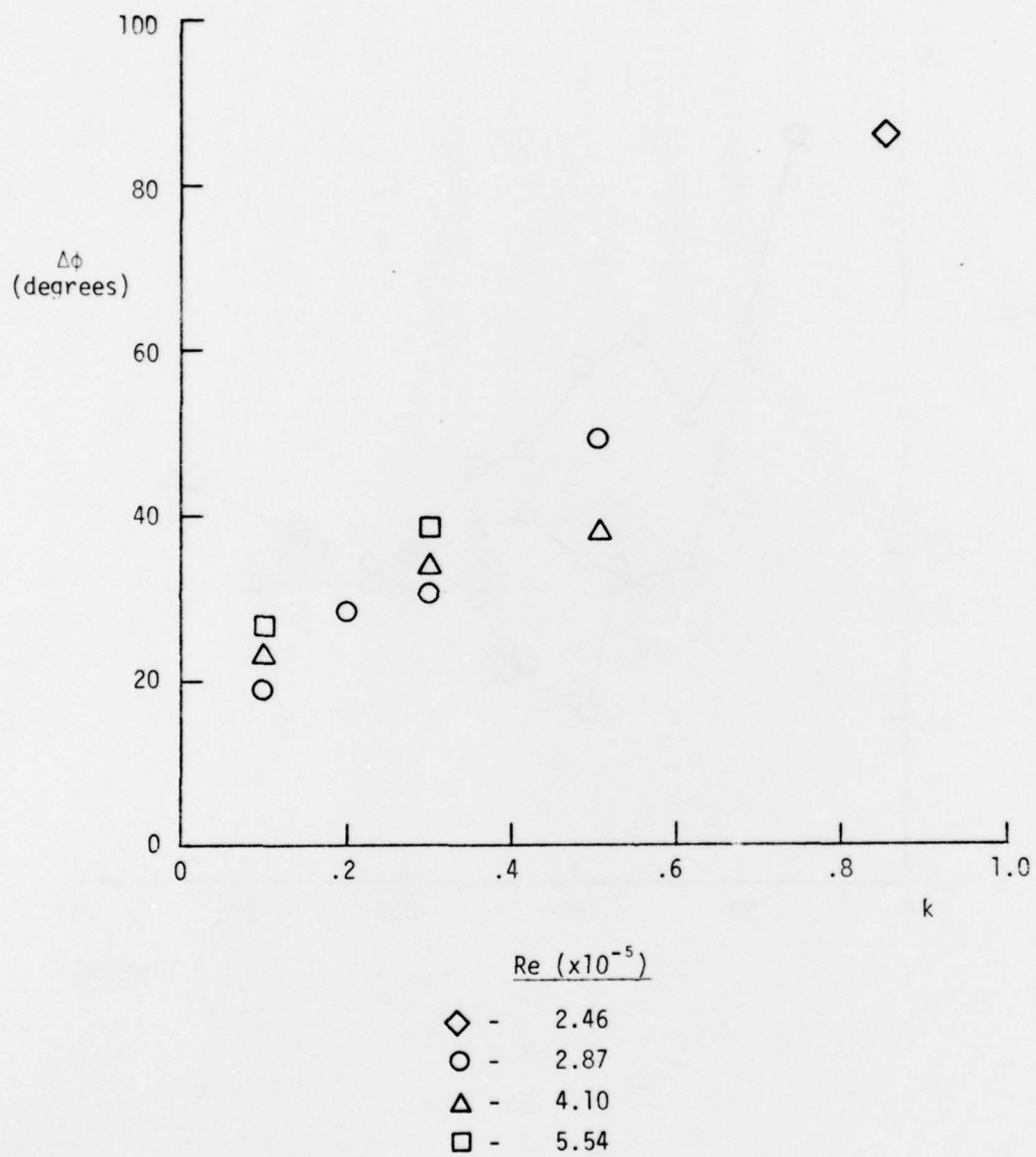
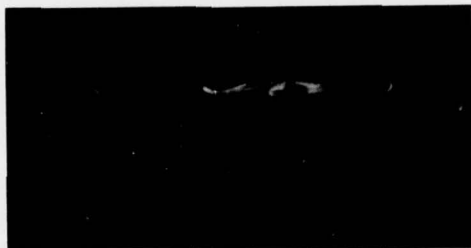
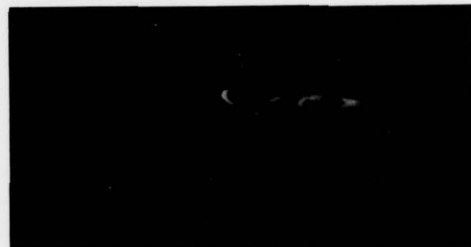


Figure 22. Phase Difference for Flow Reversal Between Electrodes 11 and 12 During Spoiler Upstroke.

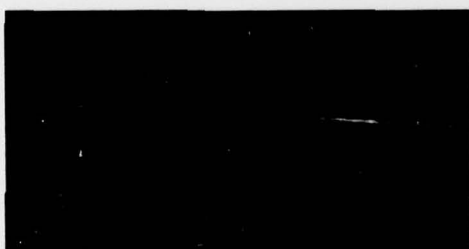


$\phi = 160^\circ$



$\phi = 180^\circ$

(a) Low Reynolds Number, $k = 5.4$, $Re = 10,000$



$\phi = 0^\circ$



$\phi = 130^\circ$



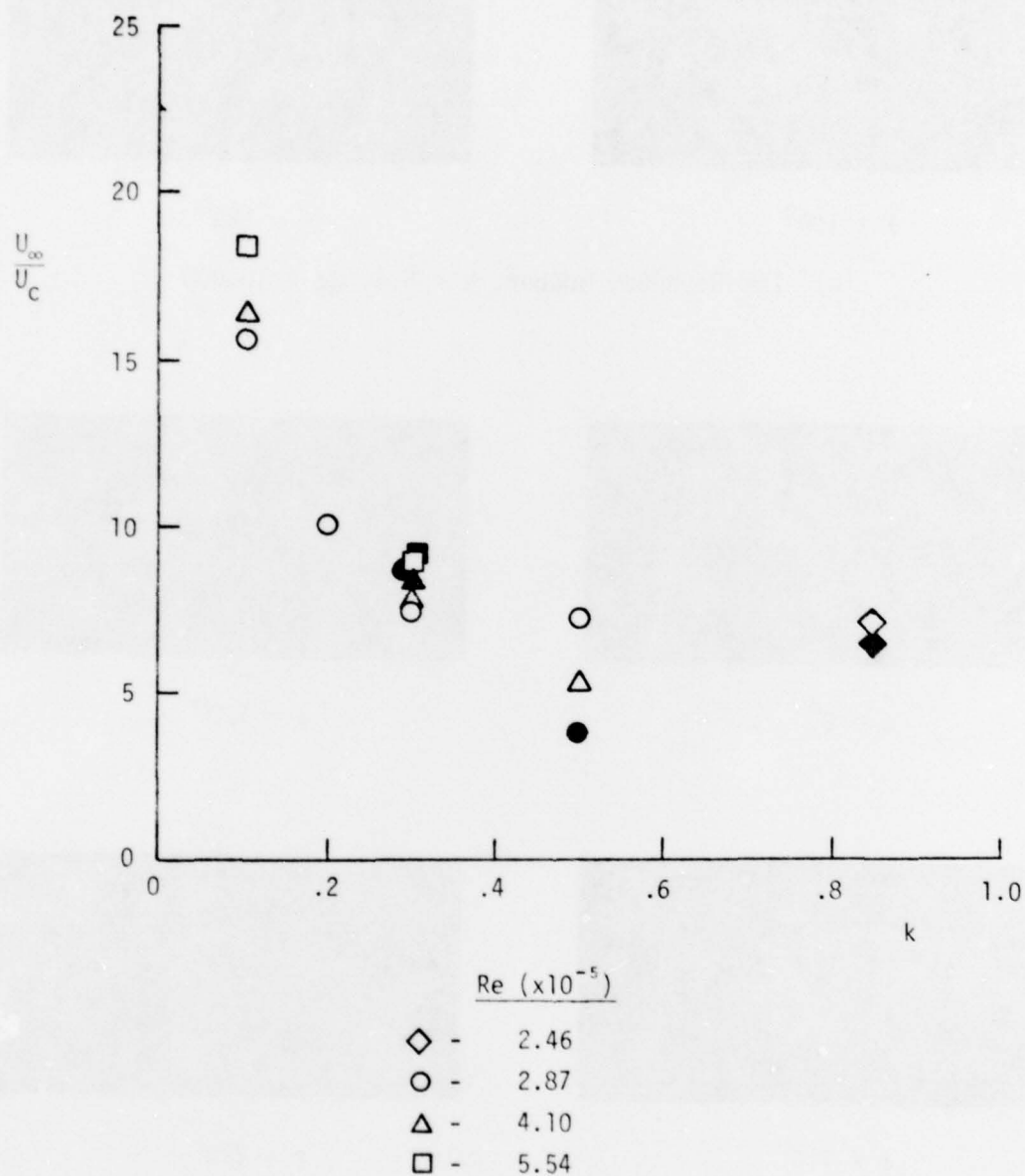
$\phi = 110^\circ$



$\phi = 220^\circ$

(b) High Reynolds Number, $k = 0.85$, $Re = 246,000$

Figure 23. Flow Reversal Near the Airfoil Surface



Open symbols denote data from flow reversal measurements;
Darkened symbols denote data obtained from measurements
of separation zone length.

Figure 24. Convective Velocity Variation with Dimensionless Frequency.

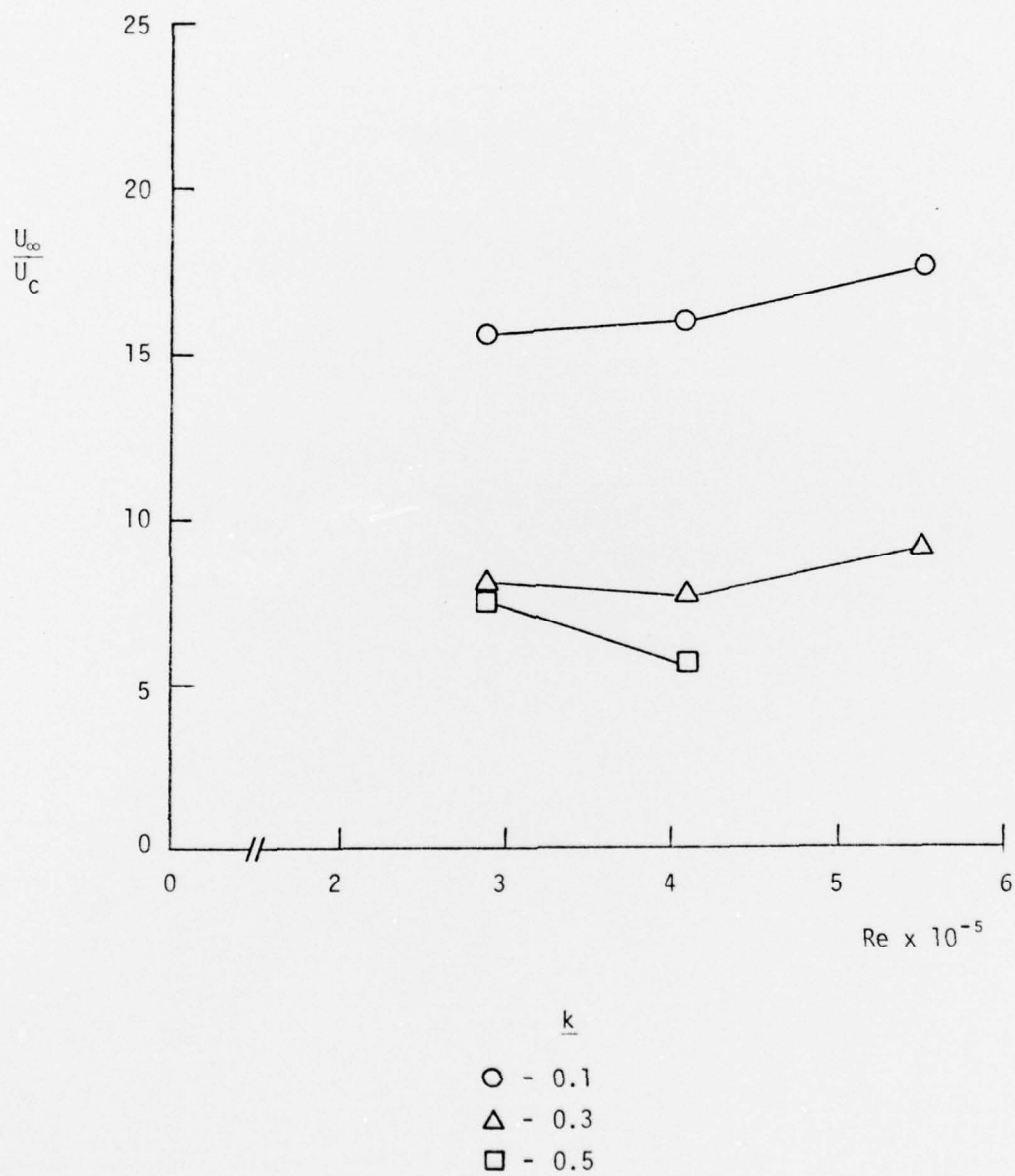


Figure 25. Convective Velocity Variation with Reynolds Number.